Enhancing reversible Na-ion intercalation by introducing K-ions into layered vanadyl phosphate for sodium-ion battery cathodes

Journal of Physics: Energy

PAPER

Enhancing reversible Na-ion intercalation by introducing K-ions into layered vanadyl phosphate for sodium-ion battery cathodes

Runzhe Wei[1], Yi Lu[1], Wanjun Ren[1], Yupei Han[1], Ajay Piriya Vijaya Kumar Saroja[1], Xueming Xia[1], Pan He[1], Charlie A F Nason[1], Zhixin Sun[2], Jawwad A Darr[1], Jiayan Luo[3], Min Zhou[2] and Yang Xu[1,*]

[1] Department of Chemistry, University College London, London WC1H 0AJ, United Kingdom
[2] Hefei National Research Centre for Physical Sciences at the Microscale, School of Chemistry and Materials Science, University of Science and Technology of China, Hefei, Anhui 230026, People's Republic of China
[3] State Key Laboratory of Metal Matrix Composites, School of Materials Science and Engineering, Shanghai Jiao Tong University, Shanghai 200240, People's Republic of China
[*] Author to whom any correspondence should be addressed.

E-mail: y.xu.1@ucl.ac.uk

Keywords: intercalation, vanadyl phosphate, pillar effect, ion exchange, interlayer expansion, cathode, sodium-ion battery

Supplementary material for this article is available online

OPEN ACCESS

RECEIVED
31 January 2024

REVISED
28 March 2024

ACCEPTED FOR PUBLICATION
8 April 2024

PUBLISHED
17 April 2024

Abstract

Vanadium-based phosphates are being extensively studied as an important family of sodium-ion battery (SIB) cathodes. Among many compositions, $NaVOPO_4$ is considered because of various polymorphs and the high redox potential of $V^{4+/5+}$. However, due to relatively poor intrinsic kinetics and electronic conductivity, approaches such as nanostructuring and carbon composites are commonly used to avoid fast performance degradation. Being different from mainstream approaches, this work utilizes the knowledge gained from potassium-ion batteries (PIBs) and applies layered $KVOPO_4$, a PIB cathode material, as a SIB cathode material. The results demonstrate that $KVOPO_4$ experiences an electrochemical K^+-Na^+ exchange during the initial cycle and a Na-dominated (de)intercalation process in the following cycles. The initial exchange results in a small amount of K^+ (~0.1 K per formula) remaining in the interlayer space and owing to the larger size of K^+ than Na^+, the residual K^+ effectively acts as 'pillars' to expand interlayer spacing and facilitates the Na (de)intercalation, leading to enhanced reversible Na storage and diffusion kinetics of $KVOPO_4$ compared to its Na counterpart $NaVOPO_4$. $KVOPO_4$ delivers an initial discharge capacity of 120 mAh g^{-1} (90% of the theoretical capacity) at 10 mA g^{-1} and retains 88% capacity after 150 cycles. It also delivers 52 mAh g^{-1} at 1 A g^{-1} and 91% capacity retention after 1000 cycles at 100 mA g^{-1}, completely outperforming $NaVOPO_4$.

1. Introduction

Lithium-ion batteries (LIBs) with high energy density and longevity have dominated energy storage applications in portable electronics and are being strongly pursued for electric vehicles [1]. However, the limited lithium and cobalt resources and consequently rising costs of the resources impose a great risk for the massively increasing demand for LIBs. Sodium-ion batteries (SIBs) are regarded as one of the most promising alternatives to LIBs with several competitive benefits, including economic benefits of the lower cost of sodium resources, potential employment of aluminum as the current collector, and good interfacial kinetics at the electrode/electrolyte interface derived from the lower desolvation energy of Na^+ in polar solvents compared with Li^+ [2–6]. Although using SIBs to replace LIBs is not immediately envisaged in the applications such as portable electronics, SIBs could play a critical role in other applications, particularly large-scale stationary energy storage where cost effectiveness and availability weight more than energy density [2, 3, 7, 8].

Vanadium-based phosphates have been extensively studied as a family of SIB cathodes, such as $Na_3V_2(PO_4)_3$ [9, 10], $NaVOPO_4$ [11–13], $NaVPO_4F$ [14, 15], and $Na_3V_2(PO_4)_2F_3$ [16, 17], because of their

high redox potentials, stable crystal structures and decent reversible capacities [18]. Among them, $NaVOPO_4$ is one of the very few that can utilize the redox pair of $V^{4+/5+}$ and achieve a high discharge voltage without the 'induction effect' of F^- or other polyanions (e.g. pyrophosphate $Na_2VOP_2O_7$ [19]). There has been increasing research on $NaVOPO_4$ as a SIB cathode material, which in partial is due to the various polymorphs of $NaVOPO_4$ and their rich intercalation chemistry. For instance, monoclinic α-phase [11] and orthorhombic β-phase $NaVOPO_4$ [12] exhibited reversible Na storage owing to the one-dimensional (1D) tunnels present in the structures; however, the 1D Na diffusion is permitted along both the *b*-axis and *c*-axis in the former but only along the *b*-axis in the latter [20]. Tetragonal/triclinic α_I-phase $NaVOPO_4$ has a layered structure that allows two-dimensional (2D) Na diffusion, which is believed to be favourable to achieve high capacity and good cycling stability [13, 20]. Although reversible Na storage is achievable in the three $NaVOPO_4$ polymorphs, Na storage performance is less ideal given the theoretical capacities of the polymorphs due to the poor Na diffusion kinetics and electronic conductivity [11, 12]. Approaches such as downsizing [13], nanostructure engineering [21], and carbon composites [12, 22] are being used to enhance Na storage performance.

Utilizing the knowledge gained from our and other groups' exploration of materials for potassium-ion batteries (PIBs) [23–31], K-containing layer-structured materials exhibit reversible K intercalation due to the larger interlayer spacings compared to their Na-containing counterparts, but they are usually formed with a lower K^+ content [32]. This is likely due to the strong K^+-K^+ repulsion in the interlayer space and consequently, not every site in the interlayer space can be occupied by the large sized K^+ [33]. As a result, these materials often show incomplete K extraction in the initial cycles, leaving a small amount of residual K^+ in the interlayer space [33–35], which has a negative impact on the performance as PIB cathodes. However, given the smaller size of Na^+ compared to K^+, the small amount of residual K^+ might expand interlayer spacing and potentially facilitate Na diffusion. Meanwhile, only a small amount of intercalation sites would be occupied by the residual K^+, potentially allowing a decent Na intercalation capacity.

In this work, we utilize layered $KVOPO_4$ (KVOP), a PIB cathode material, as a cathode material for SIBs and compare it with the Na counterpart, layered $NaVOPO_4$ (NaVOP). Our results reveal that electrochemical K^+-Na^+ exchange occurs in the initial cycle, which leads to most of the K^+ ($\sim$0.9 K per formula) in the interlayer space of KVOP being replaced by Na^+, and a small amount of residual K^+ ($\sim$0.1 K per formula) is present in the interlayer space and acts as 'pillars' in the following cycles to reduce the contraction of interlayer spacing caused by Na intercalation. Comparing to NaVOP, KVOP shows larger interlayer spacing both at charged and discharged states, because the spacing is expended by the 'pillar effect' of the residual K^+. As a result, KVOP exhibits better Na storage and kinetics as a SIB cathode, completely outperforming NaVOP. KVOP delivered an initial discharge capacity of 120 mAh g^{-1} (90% of the theoretical capacity) at 10 mA g^{-1} and retained 88% capacity after 150 cycles. The discharge capacity can be increased to 97.5% of the theoretical capacity by changing the charging condition. Also, KVOP retained 52 mAh g^{-1} at 1 A g^{-1} and 91% capacity retention after 1000 cycles at 100 mA g^{-1}. Our work takes the incomplete K extraction from KVOP, which is considered negative for PIBs, and converts it into a positive approach to develop high-performance SIB cathodes. This is different from the previously mentioned mainstream approaches to enhance Na storage and kinetics.

2. Experimental section

2.1. Materials synthesis

KVOP and NaVOP were synthesized via a two-step process. $VOPO_4 \cdot 2H_2O$ (denoted as VOP) as the precursor of the second step was synthesized by a facile reflux method. In a typical process, 4.8 g V_2O_5 and 26.6 ml 85% H_3PO_4 were dispersed in 115.4 ml H_2O. The suspension was then refluxed at 110 °C for 20 h. After refluxing, the precipitate was centrifuged and washed thoroughly by deionized water and isopropanol. VOP was obtained after overnight vacuum drying at 60 °C. KVOP and NaVOP were synthesized by chemically potassiating/sodiating VOP. For KVOP, 4.98 g KI was dissolved in 25 ml methanol. 0.625 g VOP was then added into the methanol solution. After stirring for 30 min, the suspension was transferred to a Teflon autoclave and kept at 140 °C for 12 h. The precipitate was centrifuged and washed thoroughly by deionized water and isopropanol, and then overnight vacuum dried at 60 °C. NaVOP was synthesized using the same method except for replacing KI with NaI (4.69 g). Both KVOP and NaVOP were annealed at 300 °C for 12 h in nitrogen.

2.2. Material characterizations

The crystalline structure of the powder samples was identified by an XRD diffractometer (Stoe STADI P) with Cu Kα radiation ($\lambda = 1.5406$ Å). The morphology of the powder samples was observed by a scanning electron microscope (SEM, JEOL JSM-7600F) and a transmission electron microscope (TEM, JEOL

JEM-2100). The Raman spectra of the powder samples were recorded with 633 nm laser (Renishaw Raman spectrometer). The chemical composition of the samples was collectively determined by microwave plasma atomic emission spectroscopy (MP-AES, Agilent 4210 MP-AES) and thermogravimetric analysis (TGA Discovery 5500) at a rate of 5 K min^{-1} in nitrogen. The valence state of V in the powder samples was measured by x-ray photoelectron spectroscopy (Thermoscientific Kα XPS). The XRD patterns of the electrodes were obtained by an XRD diffractometer (Panalytical Empyrean) with Cu Kα radiation ($\lambda = 1.5406$ Å). The K/Na/P ratio of the electrodes was measured by both MP-AES and energy dispersive x-ray spectroscopy (EDS) attached to the SEM.

2.3. Electrochemical measurements

Working electrodes consisted of 70 wt% active material, 20 wt% Ketjen Black (KB), and 10 wt% poly(vinylidene fluoride). The mixture was prepared into a slurry with an optimized amount of 1-methyl-2-pyrrolidone (NMP). The slurry was coated on a carbon-coated aluminum foil using a doctor blade and then vacuum dried at 120 °C overnight. The active material loading was ~1.0 mg cm^{-2}. R2032 type coin cells were assembled in an Ar-filled glovebox (water and oxygen concentrations below 1 ppm). A sodium disc was used as the counter electrode. A piece of Glass fibre filter (GF/F) was used as the separator. A solution of 1 M $NaClO_4$ dissolved in ethylene carbonate:propylene carbonate (EC:PC = 1:1 in volume) solvent was used as the electrolyte. For full-cell tests, the anode consisted of 80 wt% hard carbon (HC), 10 wt% KB, and 10 wt% carboxy methylcellulose. This mixture was prepared into a slurry with an optimized amount of deionized water. The slurry was coated on a copper foil using a doctor blade and then vacuum dried at 60 °C overnight. The HC loading was ~2.0 mg cm^{-2} and the HC anode were pre-sodiated in half-cells for 5 cycles before being applied to full-cells (N/P ratio = 4:1). Galvanostatic charge-discharge (GCD) was carried out on a Neware battery cycler (CT-4008) in a voltage range of 2.0–4.3 V (vs. Na^+/Na) at room temperature. Cyclic voltammetry (CV) was performed on a Gamry potentiostat (Interface 1010E). The fitting of peak current and square root of the scan rate was conducted using the Randles–Sevcik equation shown below [36].

$$i_p = 2.69 \times 10^5 n^{3/2} AC\sqrt{Dv}$$

where n is electron transfer number, A represents interfacial area (geometric area was used in this work), C is the concentration of ion, D is diffusion coefficient, and v is scan rate. Diffusion and capacitive behaviour were estimated by the power-law relationship between peak current and scan rate, which is shown below [37].

$$i_p = av^b$$

where a and b are adjustable constants. The b value can be obtained by linearly fitting log (i_p) versus log (v). b value of 0.5 represents a diffusion-controlled process, while b value of 1 suggests a capacitive-controlled process. Galvanostatic intermittent titration technique (GITT) measurement was carried out using a current pulse at 10 mA g^{-1} for 15 min and a 2 hour relaxation. Before the measurement, the electrodes were charged and discharged at 10 mA g^{-1} for two cycles. Na^+ diffusion coefficient was calculated based on the following equation [38].

$$D = \frac{4}{\pi\tau}\left(\frac{n_M V_M}{S}\right)^2\left(\frac{\Delta V_s}{\Delta V_t}\right)^2$$

where n_M and V_M are the molar mass and volume of the active material, respectively, τ is the time duration of current pulse, and S represents interfacial area (geometric area was used in this work). ΔV_s and ΔV_t were obtained from the GITT curves (figure S9).

3. Results and discussion

KVOP and NaVOP were synthesized through a two-step process. The layer-structured precursor VOP was first obtained by a reflux reaction, and then KVOP and NaVOP were obtained by chemically potassiating and sodiating the precursor through solvothermal reactions, respectively, where KI and NaI were used as the K and Na sources, respectively. The elemental compositions of the samples were determined by MP-AES (table S1), showing the K/V/P ratio to be 0.72/0.89/1 in KVOP and the Na/V/P ratio to be 0.85/0.86/1 in NaVOP. The ratios suggest a high degree of K/Na intercalation between the VOP layers occurred in the potassiation/sodiation reaction. The deviation of V/P ratio from the stoichiometric ratio of 1 can be attributed to a level of V/P disorder, which is not uncommon to see in V-O-P layers where a small amount of V is substituted by P [22, 39, 40]. TGA measurements were conducted to characterize the water content in

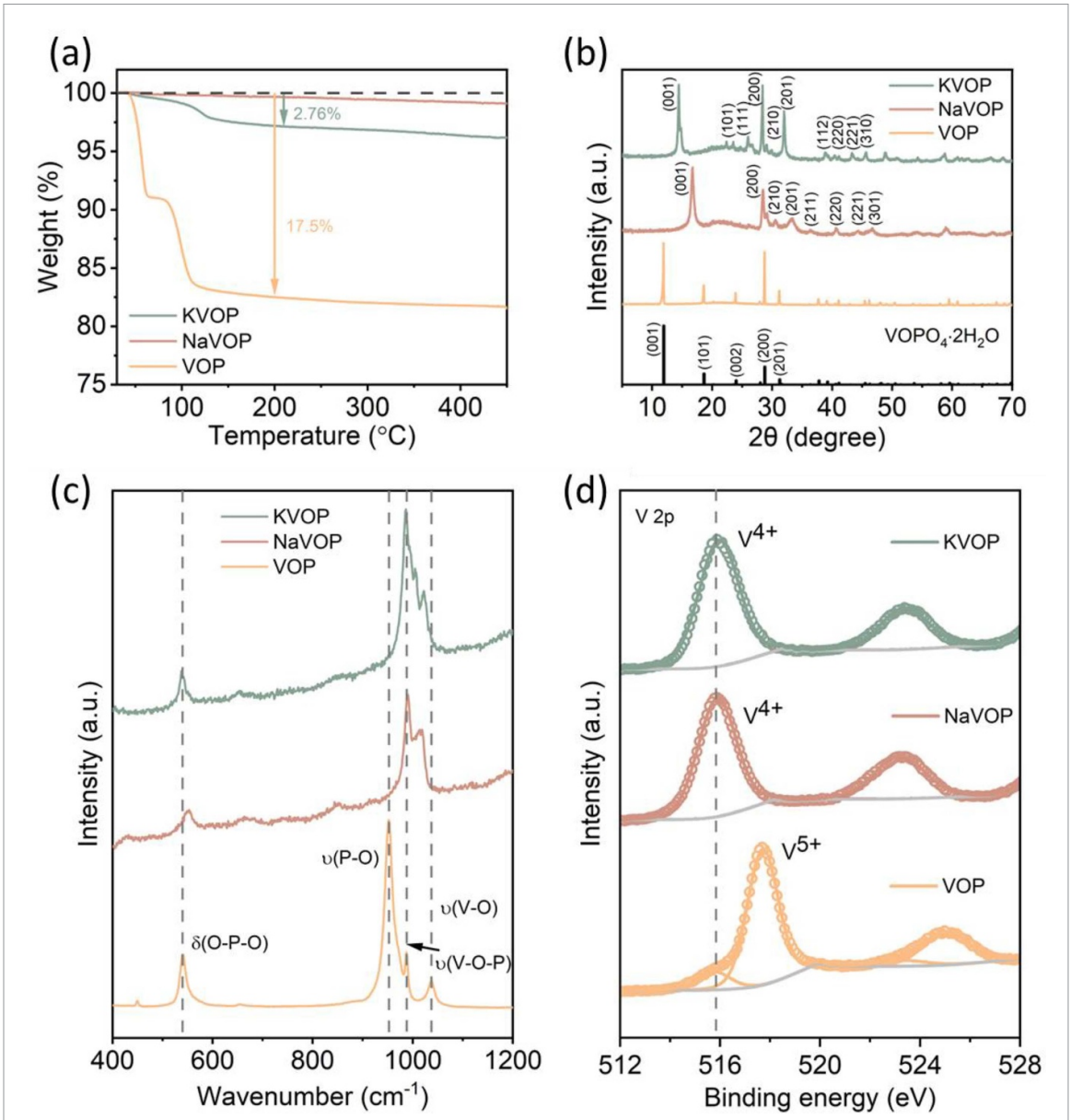

Figure 1. (a) XRD patterns, (b) TGA curves, (c) Raman spectra and (d) V 2p XPS spectra of KVOP, NaVOP and VOP.

the samples (figure 1(a)). VOP showed a weight loss of 17.5% below 200 °C, which agrees with two water molecules (18.2%) per $VOPO_4{\cdot}2H_2O$ formula [41]. KVOP showed a significantly reduced weigh loss (2.76%), while NaVOP showed almost no weight loss in the same temperature range (figure 1(a)). The contrast indicates water is substituted by K^+/Na^+ in the interlayer space of VOP during the potassiation/sodiatin reaction. The lower K ratio in KVOP than the Na ratio in NVOP could be the reason for the higher weigh loss in the former than the latter; nevertheless, a low weight loss confirms a high degree of K/Na intercalation. As shown in figure 1(b), the XRD pattern of VOP can be well indexed into $VOPO_4{\cdot}2H_2O$ (PDF#84-0111). After potassiation/sodiation, both KVOP and NaVOP can be indexed to a tetragonal structure as shown in figure 1(b). The (001) peak position shifts from 11.9° ($d = 7.41$ Å) to 14.4° ($d = 6.15$ Å) for KVOP and to 16.7° ($d = 5.29$ Å) for NaVOP, indicating the decrease of interlayer spacing, which can be ascribed to the substitution of large lattice water by K^+/Na^+ [13, 40]. Also, the reduction of V^{5+} to V^{4+} leads to negatively charged $VOPO_4$ layers, and the electrostatic attraction between the layers and K^+/Na^+ contributes to the decrease of interlayer spacing [42]. In addition, the (200) peak slightly shifts from 28.8° for VOP to 28.4° for KVOP and 28.5° for NaVOP, suggesting that K^+ and Na^+ occupying the sites between the $VOPO_4$ layers cause slight lattice expansion along the *ab* plane [20]. The XRD patterns of KVOP and NaVOP are in consistent with previously reported results, with the interlayer spacing of KVOP being between α_I-$KVOPO_4$ (6.01 Å) [43] and α_{II}-$KVOPO_4$ (6.56 Å) [40], and that of NaVOP being between 5.12 Å [22] and 5.70 Å [13]. Figure 1(c) shows the Raman spectra of KVOP, NaVOP and VOP. VOP has four peaks

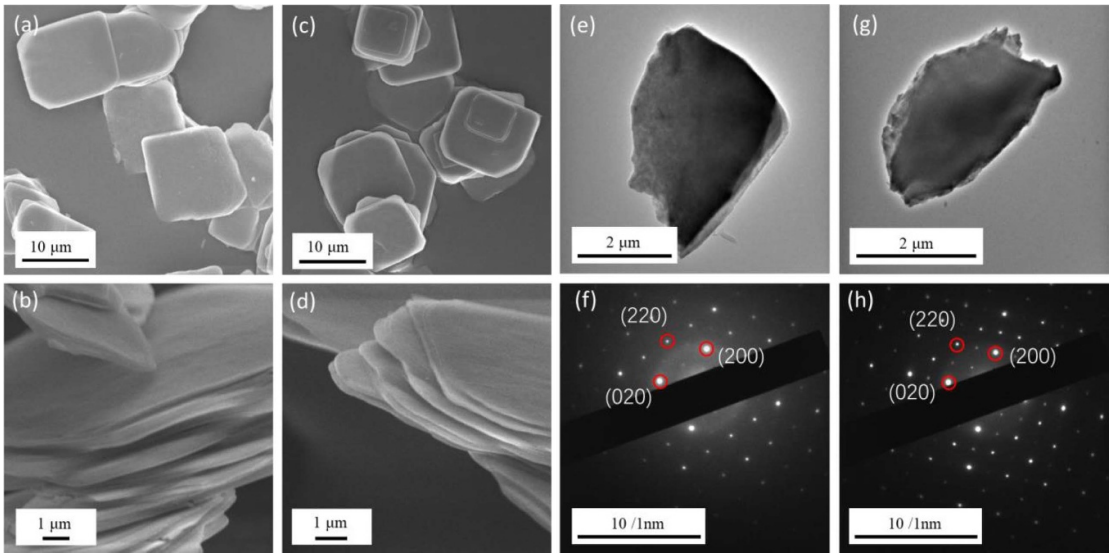

Figure 2. SEM images of (a) and (b) KVOP and (c) and (d) NaVOP. TEM images and corresponding SAED patterns of (e) and (f) KVOP and (g) and (h) NaVOP.

at 540, 953, 987 and 1037 cm^{-1}, corresponding to δ(O-P-O), υ(P-O), υ(V-O-P) and υ(V-O) vibrations, respectively [44, 45]. KVOP and NaVOP show a blue shift of υ(P-O) vibration and a red shift of υ(V-O) vibration, which indicates the strengthening of the former and the weakening of the latter due to the substitution of water with K^+ and Na^+ [13, 44]. The preservation of the characteristic peaks confirms the layered structure remained in KVOP and NaVOP. Figure 1(d) shows the V 2p XPS spectra of the samples. VOP shows a predominant peak of V^{5+} at 517.8 eV [43], with a weak shoulder peak at 517.8 eV, indicating a very small amount of V^{4+}, which is possibly due to the partial reduction of V^{5+} caused by H_3O^+ intercalation during the reflux process and/or vacuum drying process [44]. After being potassiated, KVOP shows only V^{4+} signal at 515.9 eV, due to the full reduction of V^{5+} to V^{4+} accompanied by K intercalation. Same results are seen from NaVOP. Therefore, the collective results of TGA, XRD, Raman and XPS confirm that layered KVOP and NaVOP were successfully synthesized through chemically potassiating and sodiating VOP, respectively, and their compositions were estimated to be $K_{0.77}(VO)_{0.95}(PO)_{0.05}PO_4{\cdot}0.3H_2O$ and $Na_{0.92}(VO)_{0.92}(PO)_{0.08}PO_4$.

The morphology and microstructure of the samples were examined by SEM and TEM. VOP showed a morphology of square sheet with a relatively smooth surface. The lateral size of the sheets is 7–10 μm and the thickness is in the range of 100–400 nm (figure S1); thus, the high aspect ratio reflects the layered structure of $VOPO_4{\cdot}2H_2O$. After K/Na intercalation, the square-sheet like morphology was preserved in KVOP (figures 2(a) and (b)) and NaVOP (figures 2(c) and (d)), showing no obvious morphological change, which confirms the preservation of the layered structure. The side views of KVOP (figure 2(b)) and NaVOP (figure 2(d)) show curvy edges of the sheets, which is likely due to the uneven contraction of interlayer spacing after K/Na intercalation, being consistent with literature result [13, 40, 44]. TEM measurements were taken on the KVOP and NaVOP sheets after sonication (figures 2(e) and (g)). SAED patterns demonstrate that both samples are single crystalline (figures 2(f) and (h)), as revealed by the diffraction patterns along the [001] projection which is perpendicular to the sheet plane. The (200), (020) and (220) diffractions can be clearly seen, and the angle between the (200) and (020) planes is 90° which agrees with the layered structure of VOP [44, 46], once again suggesting that the layered structure of VOP remained in KVOP and NaVOP. Using the same precursor to synthesize KVOP and NaVOP can retain the same morphological and structural features between the two, which is crucial to investigate our approach of using K-containing $KVOPO_4$ to improve the SIB performance in terms of excluding competing factors such as size, orientation, etc. This is different from previously reported approaches such as downsizing and carbon composites [13, 21, 47].

We tested KVOP and NaVOP as SIB cathodes to demonstrate the effect of having different pre-intercalated ions between the VOP layers. The electrochemical performance of Na half-cells was tested using 1 M $NaClO_4$ in EC:PC (50:50% vol.) as the electrolyte in the voltage range of 2.0–4.3 V (vs. Na^+/Na). CV curves and GCD profiles of both samples in the initial cycle are shown in figures 3(a) and (b), respectively. In the initial anodic scan, KVOP showed two oxidation peaks at 3.61 and 3.70 V, and NaVOP showed two oxidation peaks at 3.45 and 3.77 V, suggesting the initial K/Na deintercalation. Similar reduction peaks (intercalation) are seen between the two samples in the following cathodic scan, a broad peak at 3.81 V

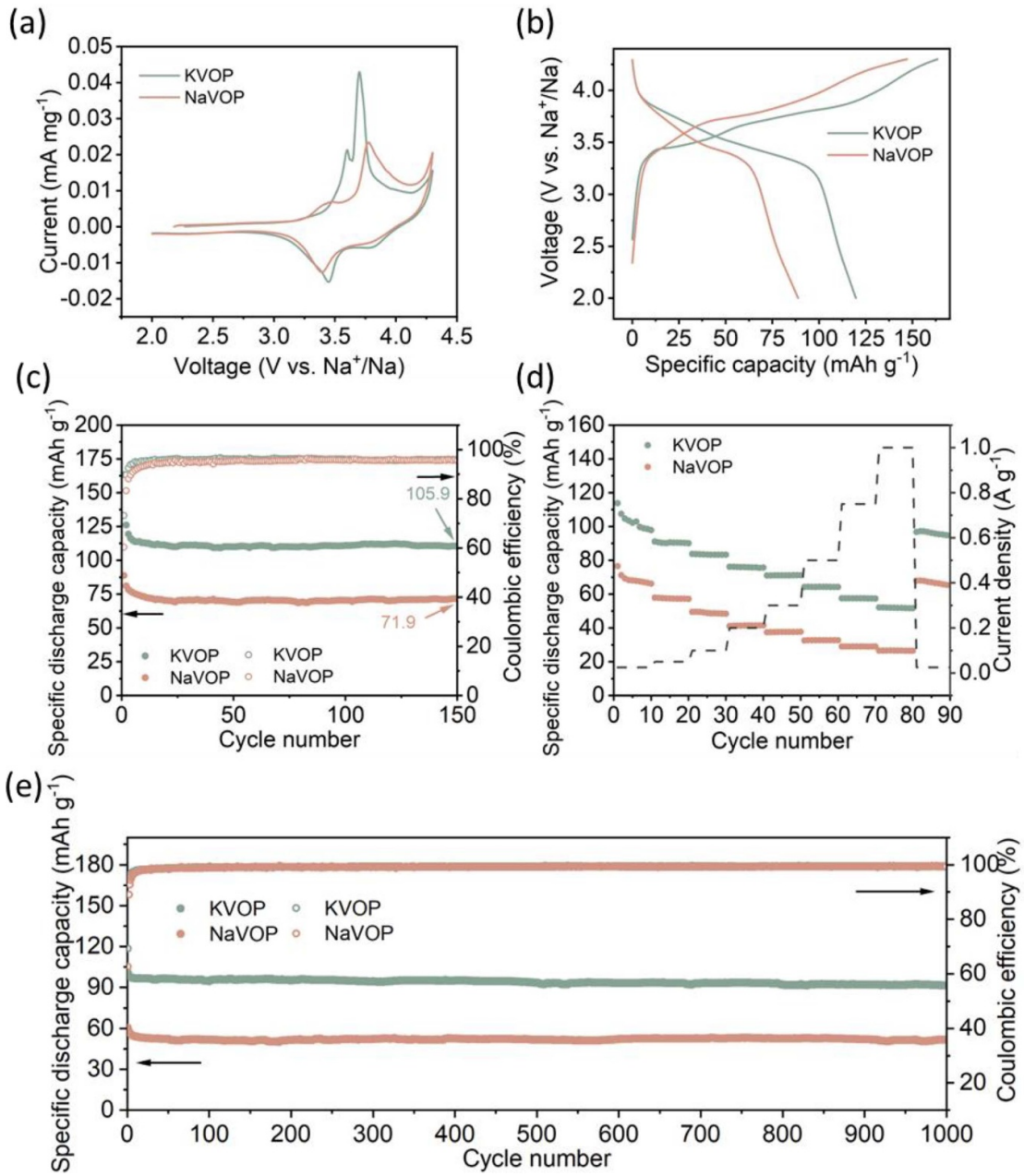

Figure 3. (a) CV curves at the scan rate of 0.02 mV s^{-1}, (b) GCD profiles and (c) cycling performance at 10 mA g^{-1}, (d) rate capability, and (e) long-term cycling performance at 100 mA g^{-1} of KVOP and NaVOP.

(KVOP)/3.77 V (NaVOP) and a strong peak at 3.44 V (KVOP)/3.39 V (NaVOP). The peak positions are in good agreement with those of $NaVOPO_4$ [13] and $Na_{0.5}VOPO_4{\cdot}2H_2O$ [48] for Na intercalation, suggesting it could be Na intercalation, not K intercalation, into KVOP and NaVOP, which in another word, indicates KVOP might experience K^+-Na^+ exchange in the first cycle in such kind of dual-ion system (K^+ in the cathode and Na^+ in the electrolyte). Interestingly, the two samples showed similar intercalation and deintercalation peaks in the 2nd and 3rd cycles (figures S2(a) and (c)), two redox pairs at 3.42/3.43 V and 3.74/3.81 V for KVOP and at 3.42/3.39 V and 3.77/3.80 V for NaVOP. This suggests Na (de)intercalation starts dominating the charge storage process in KVOP from the 2nd cycle onwards, which is an intriguing result given the different performance between KVOP and NaVOP (will be discussed later). The GCD profiles of KVOP and NaVOP are in good agreement with their respective CV curves (figure 3(b)). Both exhibited a slope discharge plateau between 3.3–3.9 V with a high average voltage of 3.5 V, which is in consistence with previous reports [13, 48]. KVOP delivered initial charge and discharge capacities of 163 and 120 mAh g^{-1}, respectively, being higher than those of NaVOP (147 mAh g^{-1} for charging and 89 mAh g^{-1} for discharging). Also, KVOP exhibited better cycling performance (figure 3(c)) and rate capability (figure 3(d)). KVOP maintained 106 mAh g^{-1} after 150 cycles at 10 mA g^{-1}, corresponding to 88% capacity retention, which was

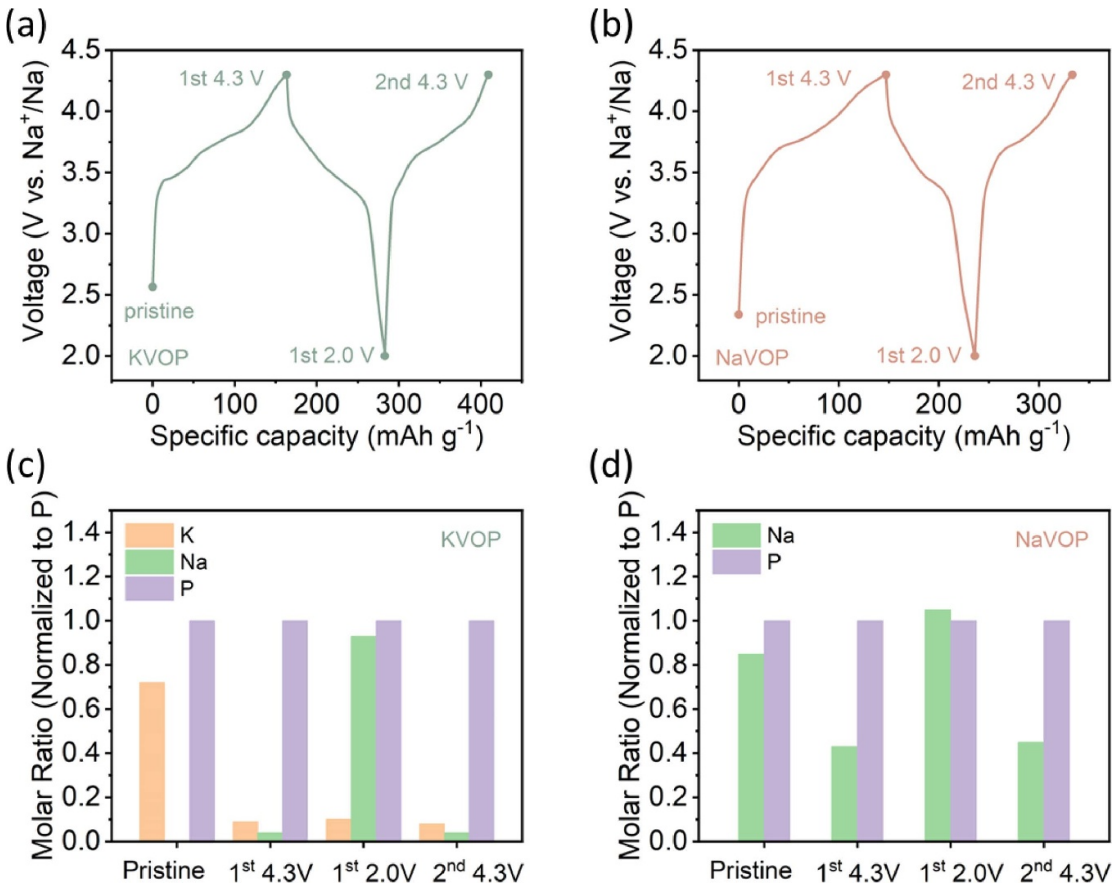

Figure 4. (a) and (b) Illustrations of the charge and discharge states of interest (a) and (b) and (c) and (d) the corresponding Na and K contents (normalized to P) measured by MP-AES in (a) and (c) KVOP and (b) and (d) NaVOP.

much higher than NaVOP (72 mAh g^{-1}, 81% retention). In terms of rate performance, KVOP delivered 107, 91, 84, 76, 71, 64, 58 and 52 mAh g^{-1} at 25, 50, 100, 200, 300, 500, 750 and 1000 mA g^{-1}, respectively, and retained 97 mAh g^{-1} when being cycled back to 25 mA g^{-1}. In contrast, NaVOP showed significant capacity fading from 71 to 41 mAh g^{-1} when the current density increased from 25 to 200 mA g^{-1}. Moreover, $<$30 mAh g^{-1} was remained at higher current densities ($\geqslant$750 mA g^{-1}). The GCD profiles at various current densities are shown in figure S3, where KVOP was able to maintain an average discharge voltage of 3.2 V even at 1000 mA g^{-1}. Furthermore, KVOP exhibited excellent long-term cyclability, retaining 91.4 mAh g^{-1} (91% capacity retention) after 1000 cycles at 100 mA g^{-1} (figure 2(e)). Therefore, KVOP completely outperformed NaVOP in reversible capacity, rate capability and cyclability. Compared to previously reported vanadyl phosphates, the KVOP cathode in this work exhibits one of the best performances (table S2), without needing to use carbon coating/composites or nanostructure engineering. As a demonstrator of high-loading electrode performance, KVOP electrode with a mass loading of 6 mg cm^{-2} were prepared and tested at 10 and 100 mA g^{-1} (figure S4). It delivered the discharge capacities of 102/95 mAh g^{-1} for the 1st/2nd cycle at 10 mA g^{-1}, being ~85% of the low-loading electrode shown in figure 3(b). Discharge capacity dropped to 82 mAh g^{-1} at 100 mA g^{-1}, being ~82% of the low-loading electrode at the same current density in figure 3(d). Given the high loading of 6 mg cm^{-2}, the capacities kept reasonably well.

The CV and GCD profiles strongly suggest that the intercalation processes of KVOP and NaVOP are highly similar, and therefore, the presence of K^+ between the VOP layers should have a crucial role in improving Na storage performance. Thus, we drew our attention to the K/Na (de)intercalation processes of the samples by measuring the K/Na content (normalized to P) in the KVOP and NaVOP cathodes at various states of charge and discharge. The states of interest are illustrated in figures 4(a) and (b) for KVOP and NaVOP, respectively, and the measurement was carried out using both MP-AES (figures 4(c) and (d)) and EDS (tables S3, S4 and figures S5, S6). The results of the two measurements agreed with each other. As shown in figure 4(c), the K content in KVOP decreases from 0.72 per formula in the pristine state to 0.09 per formula at the end of the 1st charge (1st 4.3 V), meaning 87.5% of K^+ is extracted. It is interesting that, in the following discharge to 2.0 V (1st 2.0 V), Na content significantly increases to 0.93 (~90% Na intercalation per formula), but no obvious K intercalation is observed as K content remains unchanged.

Thus, K^+-Na^+ exchange occurs in the initial cycle, and ~0.1 K per formula stays in the interlayer space, which effectively results in $K_{0.1}Na_{0.9}VOP$ being the working cathode material. The deintercalated K^+ stays in the electrolyte and does not intercalate back into KVOP, which has been seen in previous work [49]. This is further supported by the ~90% Na deintercalation per formula at the end of the following charge (2nd 4.3 V) and the almost unchanged K content (0.08 per formula). The results suggest that Na dominates the (de)intercalation process in KVOP, contributing a capacity equivalent to ~0.9 Na per formula, and the residual 0.1 K after the initial charge does not participate in the (de)intercalation process but acts as 'pillars' in the interlayer space, which facilitates Na intercalation (will be further discussed later). Compared to KVOP, NaVOP shows an expected Na (de)intercalation process (figure 4(d)) without the presence of K^+ in the cell. Na content decreases to 0.43 per formula after initial charge (1st 4.3 V), increases to ~1.0 after the initial discharge (1st 2.0 V), and falls back to 0.45 after the following charge (2nd 4.3 V), giving rise to ~0.6 Na intercalation per formula wand ~0.4 Na being 'stuck' between the VOP layers. It can be concluded that the residual K (~0.1 per formula) between the VOP layers leads to the formation of $K_{0.1}Na_{0.9}VOP$ after the initial cycle and improves Na storage, resulting in a higher amount of reversible Na intercalation in $K_{0.1}Na_{0.9}VOP$ than NaVOP (0.9 vs. 0.6 per formula) and thus a higher reversible capacity (106 vs. 72 mAh g^{-1}). Furthermore, due to the larger size of K^+ than Na^+, the residual 0.1 K not only expands interlayer spacing but also keeps it expanded during cycles, and as a result, better Na diffusion kinetics is obtained in $K_{0.1}Na_{0.9}VOP$ compared to NaVOP, leading to enhanced rate capability. Based on the above discussion, the reaction mechanism of KVOP can be described by equations (1) and (2), and the reaction mechanism of NaVOP can be described by equations (3) and (4)

$$\text{First charge}: K_{0.77}VOPO_4 - 0.67K^+ - 0.67e^- \rightarrow K_{0.1}VOPO_4 \quad (1)$$

$$\text{Following charge/discharge}: K_{0.1}VOPO_4 + 0.9Na^+ + 0.9e^- \leftrightarrow Na_{0.9}K_{0.1}VOPO_4 \quad (2)$$

$$\text{First charge}: Na_{0.92}VOPO_4 - 0.52Na^+ - 0.52e^- \rightarrow Na_{0.4}VOPO_4 \quad (3)$$

$$\text{Following charge/discharge}: Na_{0.4}VOPO_4 + 0.6Na^+ + 0.6e^- \leftrightarrow Na_1VOPO_4. \quad (4)$$

We then investigated the interlayer spacing change of the two samples during the initial cycles (figures 5(a) and (c)) to further illustrate the role of the residual K^+ in KVOP. As shown in figure 5(b), the (001) peak of KVOP slightly shifts from 14.4° ($d = 6.15$ Å) to 14.8° ($d = 5.98$ Å) at the beginning of K deintercalation (pristine → state 1), which is possibly due to the phase transition from α_{II}-$KVOPO_4$ to α_I-$KVOPO_4$ [40]. A shoulder peak at 13.6° ($d = 6.48$ Å) can be detected, and its position is very close the (001) peak of $K_{0.5}VOPO_4{\cdot}1.5H_2O$ (13.8°, $d = 6.38$ Å, PDF#07-3345, figure S7), suggesting that a K-deficient phase might start forming [50]. When further charged, the original (001) peak gradually disappears, and the shoulder peak gradually becomes the dominant (001) peak while shifting to a lower angle, due to the weakened electrostatic attraction between the $VOPO_4$ layers during K deintercalation. At the end of charge (state 3), the (001) peak appears at 13.0° ($d = 6.80$ Å), which is close to the de-potassiated K_xVOPO_4 reported in PIBs [40, 50]. During the following discharge (Na intercalation as discussed previously), the (001) peak shifts back to 16.5° ($d = 5.37$ Å, state 6), forming a Na-rich phase $K_{0.1}Na_{0.9}VOP$ [51]. The d value is smaller than the one before cycling ($d = 6.15$ Å) because of the smaller size of Na^+ than K^+. In the following charge (Na de-intercalation), the peak moves back to 13.0° (state 7), the same position at the end of the first charge (state 3), which evidences the existence of the residual K^+ in the interlayer space, even though different cations are deintercalated during the first (K^+) and second (Na^+) charge. This in turn solidifies the 'pillar effect' provided by the stable residual K^+ and the resultant reversible ~0.9 Na (de)intercalation per formula in KVOP (figure 4(c)). The XRD patterns of NaVOP are shown in figure 5(d). During the initial charge (pristine → state 3), the strong (001) peak at 16.8° ($d = 5.26$ Å) remains almost unshifted. A weak peak at 13.6° ($d = 6.54$ Å), which is close to the (001) peak of $Na_{0.5}VOPO_4{\cdot}2H_2O$ (PDF#70-4607, figure S7), appears at state 2, and its intensity increases at state 3 (end of charge). The splitting of the peaks indicates that two phases, possibly a Na-rich phase and a Na-deficient phase, may form and be present throughout Na deintercalation [13, 52], which echoes the observation of the incomplete Na deintercalation (figure 4(d)), ~0.4 Na per formula being 'stuck' in the interlayer space. In the following discharge (state 3 → state 6) and charge (state 6 → state 7), the peak at 13.6° reversibly decreases (discharge) and increases (charge), corresponding to the reversible disappearance and appearance of the second phase, respectively. Despite that KVOP and NaVOP show somewhat reversible XRD peak shifts, it is worth emphasizing that KVOP has a larger interlayer space than NaVOP at both end-charge (6.80 Å vs. 6.54/5.26 Å) and end-discharge states (5.37 Å vs. 5.26 Å), which once again proves the advantage of KVOP over NaVOP in

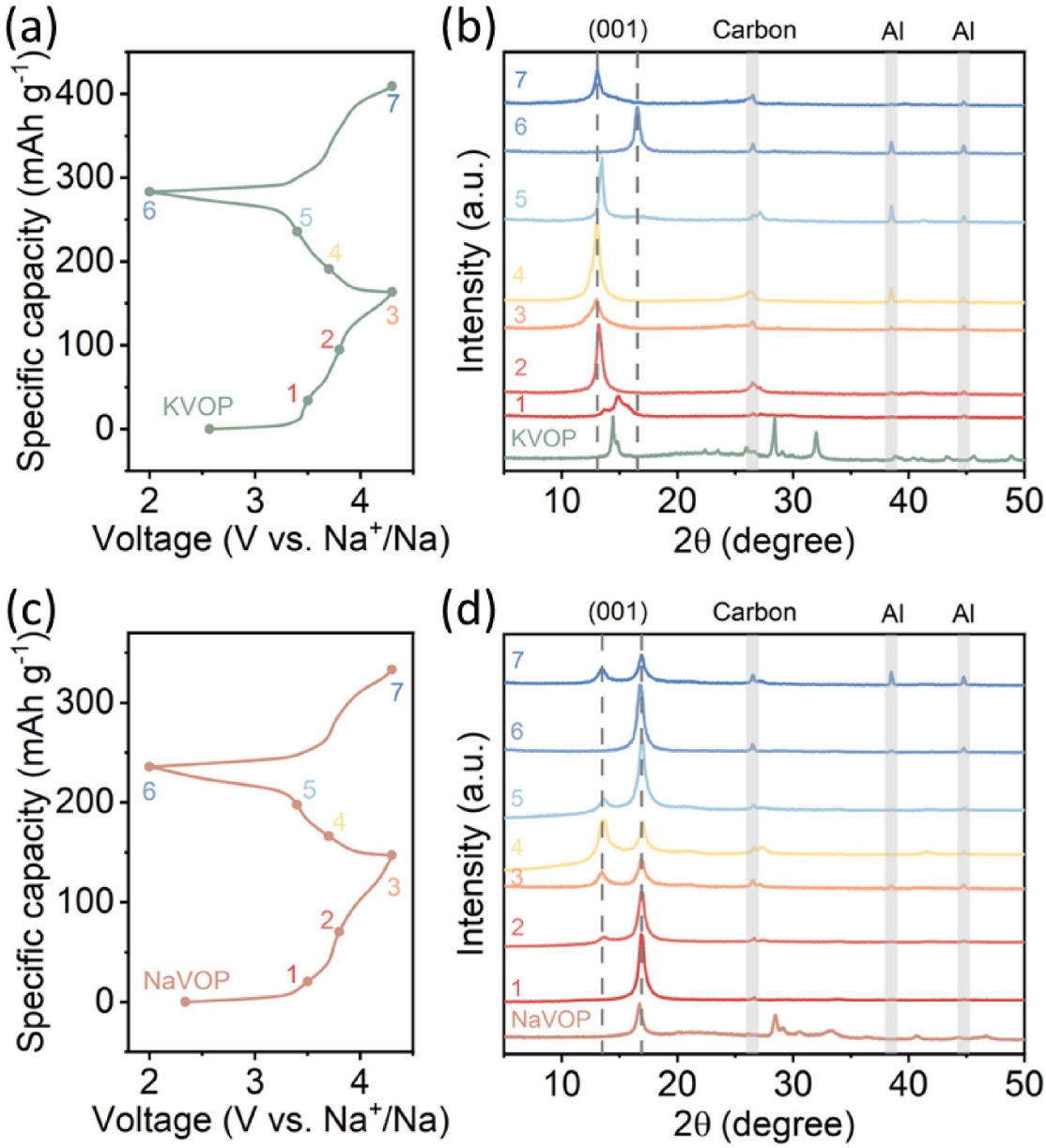

Figure 5. (a) and (c) Illustrations of the charge and discharge states of interest and (b) and (d) the corresponding XRD patterns of (a) and (b) KVOP and (c) and (d) NaVOP.

terms of delivering a higher reversible Na capacity and realizing better Na diffusion kinetics, due to the stable residual K^+ in the former, i.e. the 'pillars'.

In addition, we carried out experiments to further verify the 'pillar effect' of K^+ by changing the amount of residual K^+ in the interlayer space. On the one hand, we lowered the cut-off charging voltage to 4.0 V to retain more residual K^+, and on the other hand, we added a constant-voltage step after the constant-current charge (CCCV) to 4.3 V so that more K^+ can be extracted, i.e. less residual K^+ is retained. With the cut-off voltage at 4.0 V (figure 6(a)), both KVOP and NaVOP exhibited lower initial capacities of 111 and 70 mAh g^{-1}, respectively, compared to the cut-off voltage of 4.3 V (figure 3(b)), because less K^+ and Na^+ deintercalated and thus less Na^+ intercalated afterwards. The fact that KVOP delivered a higher capacity than NaVOP throughout cycles shows that increasing residual K^+ in KVOP has the same beneficial role in increasing Na intercalation capacity compared to NaVOP. As shown in figure 6(b), adding a constant-voltage charging step results in a reduced K/P ratio in KVOP (0.06 at CCCV vs. 0.09 at CC, table S3) and Na/P ratio in NaVOP (0.35 at CCCV vs. 0.43 at CC, table S4), suggesting a reduced amount of residual K^+. Still, KVOP

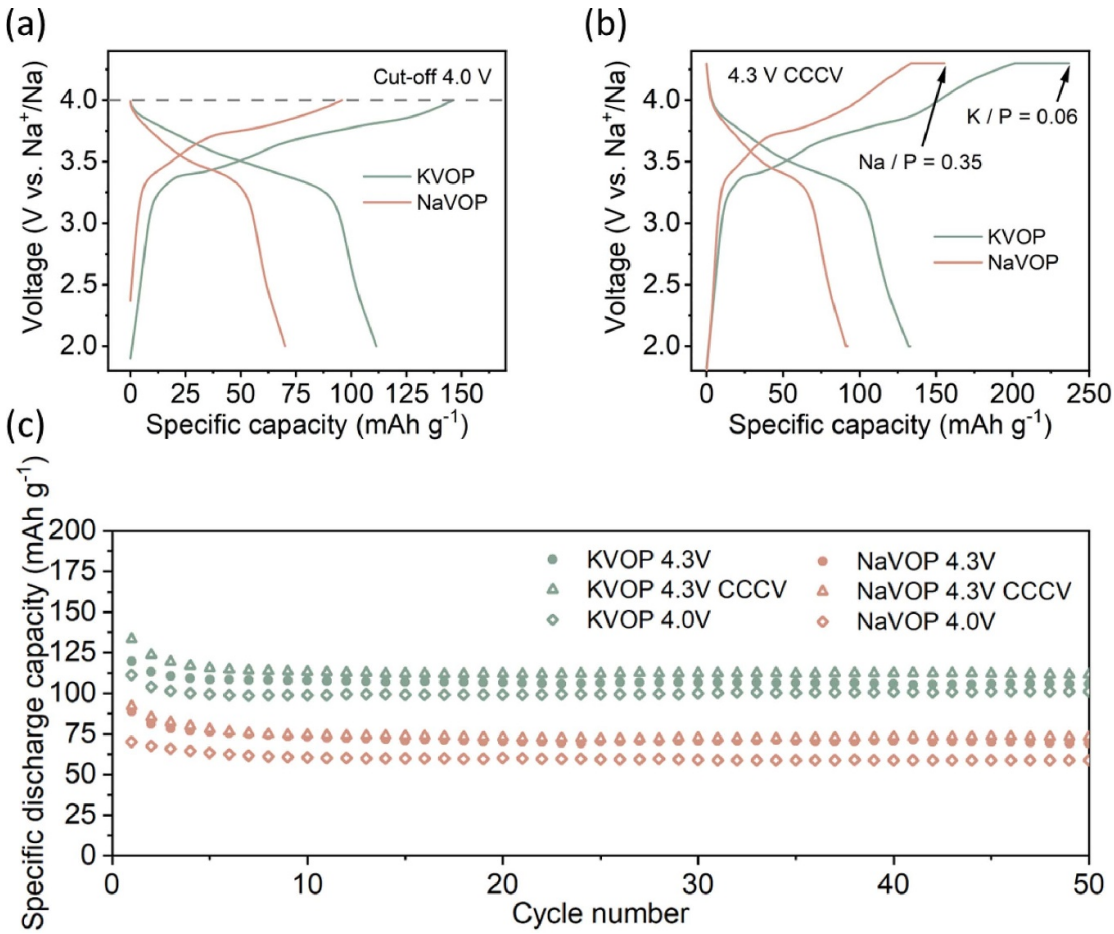

Figure 6. GCD profiles of the first cycle between 2.0–4.0 V at 10 mA g^{-1} (a) and between 2.0–4.3 V with the CCCV mode at 10 mA g^{-1} (b) of KVOP and NaVOP. (c) Cycling performance over 50 cycles at both charging conditions.

delivered a higher discharge capacity than NaVOP (130 vs. 92 mAh g^{-1}), with the capacity being close to its theoretical capacity (assuming 1e transfer per $KVOPO_4$). The increase in capacity sustained in the following cycle (figure S8) and over 50 cycles (figure 6(c)) at both charging conditions. Therefore, the additional experiments verify that the beneficial role of the residual K^+ in KVOP in improving Na storage compared to NaVOP is not dependent on the amount of the residual K^+.

Moreover, we carried out measurements to investigate electrochemical kinetics, further demonstrating the enhancement enabled by the 'pillar effect' of K^+ in KVOP for Na storage. CV tests at various scan rates from 0.02 to 0.5 mV s^{-1} were carried out to obtain the diffusion coefficient of KVOP and NaVOP (figures 7(a) and (b)). All the reduction and oxidation peaks were identifiable and reversible with no obvious peak shape change, showing no significant side reactions during the Na (de)intercalation at high scan rates [53]. The potential differences of the reduction/oxidation peaks increased to a small extent when increasing the scan rate. The linear relationship between the peak current and the square root of the scan rate was fitted by the Randles-Sevcik equation (figures 7(c) and (d)). The diffusion coefficients of KVOP were calculated to be 4.8×10^{-12} and 2.4×10^{-12} cm^2 s^{-1} for the reduction and oxidation peaks, respectively, which were 4–6 times higher than those of NaVOP, being 1.1×10^{-12} (reduction) and 3.8×10^{-13} cm^2 s^{-1} (oxidation). The linear relationship between the log (peak current) and log (scan rate) was fitted to obtain *b* values (figures 7(e) and (f)). KVOP and NaVOP showed similar *b* values of 0.74/0.72 and 0.76/0.71 for reduction and oxidation peaks, respectively, suggesting the Na storage process between the two samples are similar and not altered by the 'pillar effect'. Additionally, diffusion coefficients were measured by GITT (figures 7(g) and (h)). In general, KVOP exhibited smaller overpotentials than NaVOP, especially at the sloping plateau region. The diffusion coefficient of KVOP was calculated (figure S9) in the range of 10^{-10}–10^{-12} cm^2 s^{-1}, which was about one magnitude higher than that of NaVOP (10^{-11}–10^{-13} cm^2 s^{-1}). The results of diffusion coefficient from CV and GITT agree reasonably well with each other. Therefore, the enlarged interlayer space

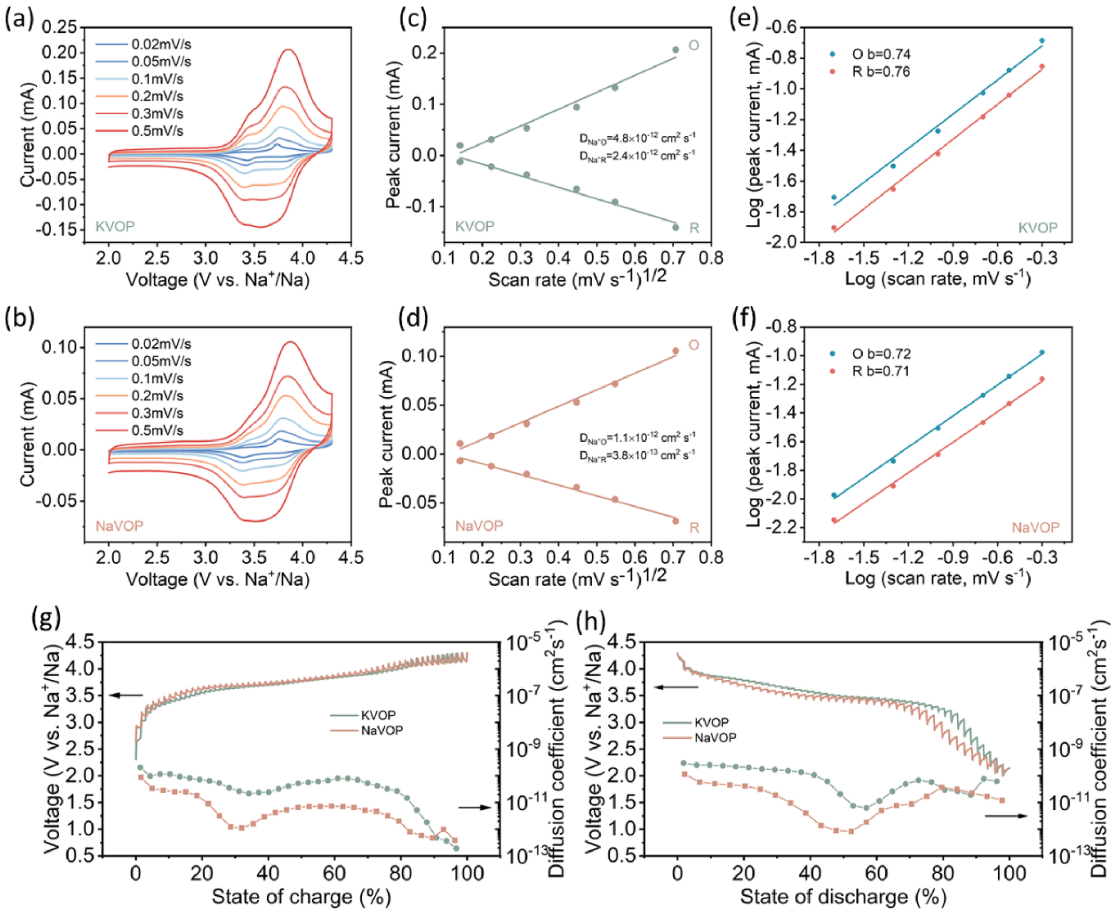

Figure 7. (a) and (b) CV curves at various scan rates, (c) and (d) the corresponding linear fitting between the peak current and the square root of the scan rate, and (e) and (f) between log peak current and log scan rate of (a), (c) and (e) KVOP and (b), (d) and (f) NaVOP. GITT curves and the calculated diffusion coefficients of KVOP and NaVOP during (g) charge and (h) discharge.

due to the 'pillar effect' of the residual K^+ can facilitate Na^+ diffusion in KVOP, leading to an enhanced rate capability in comparison to NaVOP.

Finally, we demonstrated the application of KVOP as a SIB cathode in full-cells (figure S10) by paring it with hard carbon (HC). The KVOP||HC full-cell delivered initial charge and discharge capacities of 187 and 125 mAh g^{-1} at 10 mA g^{-1}, respectively (figure S8(b)). A sloping discharge plateau within 3.9–3.0 V was observed. The capacity is comparable to the KVOP half-cell capacity, and the sloping discharge plateau is in a reasonable voltage range, considering the charge voltage of HC. In term of cycling stability, the full-cell was able to retain 107 mAh g^{-1} after 150 cycles at 10 mA g^{-1}, corresponding to a capacity retention of 86%. In addition, the full cell delivered discharge capacities of 94, 81, 74, 68, 64, 59 and 54 mAh g^{-1} at 25, 50, 100, 200, 300, 500, and 750 mA g^{-1}, respectively. Comparing to the half-cell, the capacities were ∼10% less at the current densities between 25–200 mA g^{-1} and kept well at the current density of 300 mA g^{-1} onwards.

With the above results and discussion, we illustrate in figure 8 the benefit of using KVOP as a SIB cathode in comparison to using NaVOP. In the case of NaVOP (figure 8(b)), due to the smaller initial interlayer spacing (d) and sluggish Na^+ diffusion, it is suffered from incomplete Na deintercalation in the initial charge, which results in a lower capacity and worse rate capability compared to KVOP (figures 3(c) and (d)). In contrast, KVOP has a larger initial d, and more K^+ deintercalated from KVOP in the initial charge than Na^+ from NaVOP (figure 8(a)), which allows more Na^+ to reversibly (de)intercalate in the following cycles (figures 4(c) and (d)). The performance enhancement of KVOP is originated from ∼0.1 K per formula remaining between the VOP layers after the initial charge, essentially acting as 'pillars' to expand d at both charged and discharged states, whereas, despite there is Na^+ remaining between the VOP layers due to the incomplete Na deintercalation, the smaller size of Na^+ than K^+ cannot expand d in NaVOP to the same extent as in KVOP (figures 5(b) and (d)). Therefore, introducing K^+ into layer-structured cathode materials of SIBs can be a facile and effective approach to boost Na storage performance.

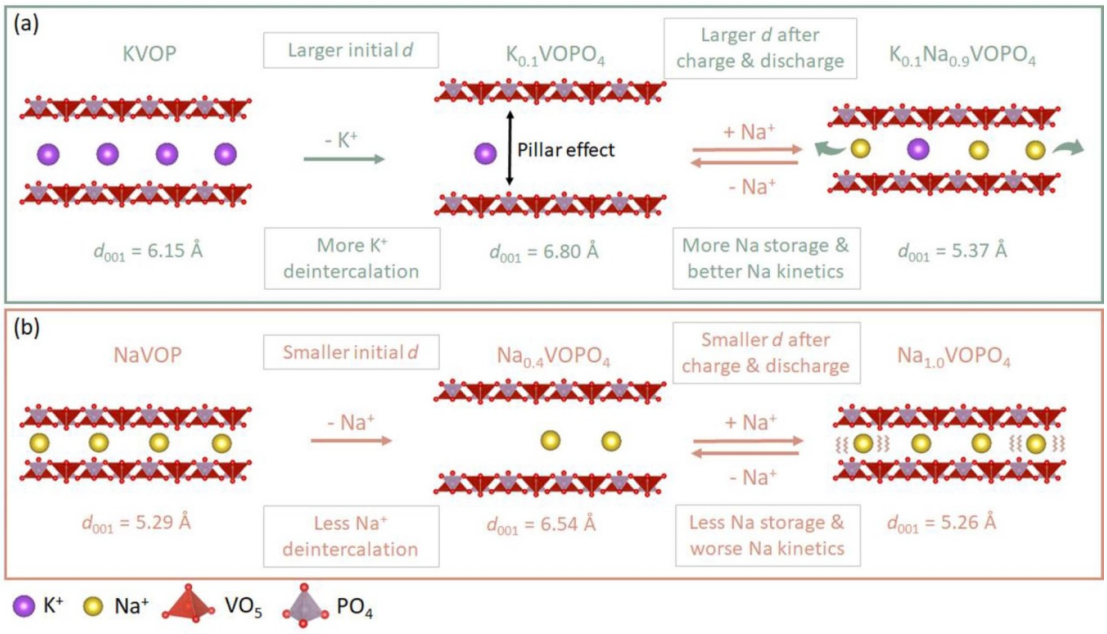

Figure 8. Schematic illustration of Na/K (de)intercalation in KVOP (a) and NaVOP (b) when both are used as cathode materials in SIBs.

4. Conclusions

In summary, we carried out a study on the electrochemical performance, cation intercalation mechanism, interlayer spacing evolution and cation diffusion kinetics of the KVOP cathode to understand how the presence of larger sized K^+ effects the storage and kinetics of smaller sized Na^+ in SIBs. Our study reveals that the residual K^+ between the VOP layers after the initial charge process induces a 'pillar effect' that keeps the interlayer spacing expanded throughout the following Na (de)intercalation process. This not only increases reversible Na storage capacity but also improves Na diffusion kinetics. Owing to the effect, KVOP outperformed NaVOP in terms of reversible capacity and rate capability. $VOPO_4$ is a promising SIB cathode material due to its layered structure, and interlayer engineering is an effective way to enhance its performance; however, the straightforwardness of interlayer engineering is crucial. This work does not follow mainstream approaches and provides an interesting one to 'in-situ' engineer the interlayer of VOP via introducing a larger sized ion into interlayer space of the pristine material and utilize the large size of the ion to assist the intercalation and diffusion of a smaller sized ion; the readiness of our approach is evidenced. We believe our approach could be general to other ion batteries based on intercalation chemistry, particularly the batteries that face the challenges of insufficient ion accessibility and slow ion diffusion, such as multivalent-ion batteries.

Data availability statement

All data that support the findings of this study are included within the article (and any supplementary files).

Acknowledgments

Y X acknowledges the financial support of the Engineering and Physical Sciences Research Council (EP/X000087/1, EP/V000152/1), Leverhulme Trust (RPG-2021-138), Royal Society (IEC\NSFC\223016), and Science and Technology Facilities Council Batteries Network (ST/R006873/1), and UCL Global Partner Funds. The authors thank Deregellera Ltd (UK) for providing hard carbon anode materials for the full-cell measurements. For the purpose of open access, the author has applied for a Creative Commons Attribution (CC BY) license to any author-accepted manuscript version arising.

ORCID iDs

Min Zhou https://orcid.org/0000-0003-2677-5472
Yang Xu https://orcid.org/0000-0003-0177-6348

References

[1] Olabi A G, Abbas Q, Shinde P A and Abdelkareem M A 2022 *Energy* **266** 126408
[2] Berg E J, Villevieille C, Streich D, Trabesinger S and Novák P 2015 *J. Electrochem. Soc.* **162** A2468
[3] Larcher D and Tarascon J-M 2015 *Nat. Chem.* **7** 19–29
[4] Yabuuchi N, Kubota K, Dahbi M and Komaba S 2014 *Chem. Rev.* **114** 11636–82
[5] Zhang Q, Wang Z, Zhang S, Zhou T, Mao J and Guo Z 2018 *Electrochem. Energy Rev.* **1** 625–58
[6] Rudola A, Wright C J and Barker J 2021 *Energy Mater. Adv.* **2021** 9798460
[7] Wang Q, Li J, Jin H, Xin S and Gao H 2022 *InfoMat* **4** e12311
[8] Zhu Y F, Xiao Y, Dou S X, Kang Y M and Chou S L 2021 *eScience* **1** 13–27
[9] Jian Z, Han W, Lu X, Yang H, Hu Y S, Zhou J, Zhou Z, Li J, Chen W and Chen D 2013 *Adv. Energy Mater.* **3** 156–60
[10] Saravanan K, Mason C W, Rudola A, Wong K H and Balaya P 2013 *Adv. Energy Mater.* **3** 444–50
[11] Song J, Xu M, Wang L and Goodenough J B 2013 *Chem. Commun.* **49** 5280–2
[12] Ni Y and He G 2018 *Electrochim. Acta* **292** 47–54
[13] Fang Y, Liu Q, Xiao L, Rong Y, Liu Y, Chen Z, Ai X, Cao Y, Yang H and Xie J 2018 *Chem* **4** 1167–80
[14] Barker J, Saidi M and Swoyer J 2002 *Electrochem. Solid-State Lett.* **6** A1
[15] Shraer S D, Luchinin N D, Trussov I A, Aksyonov D A, Morozov A V, Ryazantsev S V, Iarchuk A R, Morozova P A, Nikitina V A and Stevenson K J 2022 *Nat. Commun.* **13** 4097
[16] Shakoor R, Seo D H, Kim H, Park Y U, Kim J, Kim S W, Gwon H, Lee S and Kang K 2012 *J. Mater. Chem.* **22** 20535–41
[17] Liu Q, Wang D, Yang X, Chen N, Wang C, Bie X, Wei Y, Chen G and Du F 2015 *J. Mater. Chem.* A **3** 21478–85
[18] Li H, Xu M, Zhang Z, Lai Y and Ma J 2020 *Adv. Funct. Mater.* **30** 2000473
[19] Barpanda P, Liu G, Avdeev M and Yamada A 2014 *ChemElectroChem* **1** 1488–91
[20] Aparicio P A, Dawson J A, Islam M S and De Leeuw N H 2018 *J. Phys. Chem.* C **122** 25829–36
[21] Shen X, Han M, Li X, Zhang P, Yang C, Liu H, Hu Y-S and Zhao J 2022 *ACS Appl. Mater. Interfaces* **14** 6841–51
[22] He G, Kan W H and Manthiram A 2016 *Chem. Mater.* **28** 682–8
[23] Nason C A, Vijaya Kumar Saroja A P, Lu Y, Wei R, Han Y and Xu Y 2024 *Nano-Micro Lett.* **16** 1
[24] Vijaya Kumar Saroja A P, Wang Z, Tinker H R, Wang F R, Shearing P R and Xu Y 2023 *SusMat* **3** 222–34
[25] Han J, Li G N, Liu F, Wang M, Zhang Y, Hu L, Dai C and Xu M 2017 *Chem. Commun.* **53** 1805–8
[26] Park W B, Han S C, Park C, Hong S U, Han U, Singh S P, Jung Y H, Ahn D, Sohn K S and Pyo M 2018 *Adv. Energy Mater.* **8** 1703099
[27] Wei R, Zhai X, Tinker H R, He P, Nason C A F, Han Y, Celorrio V, Sankar G, Zhou M and Xu Y 2023 *Adv. Funct. Mater.* **33** 2308227
[28] Zhang C, Xu Y, Zhou M, Liang L, Dong H, Wu M, Yang Y and Lei Y 2017 *Adv. Funct. Mater.* **27** 1604307
[29] Nason C A and Xu Y 2023 *eScience* **4** 100183
[30] Xu Y, Titirici M, Chen J, Cora F, Cullen P L, Edge J S, Fan K, Fan L, Feng J and Hosaka T 2023 *J. Phys. Energy* **5** 021502
[31] Wang M, Wang Q, Ding X, Wang Y, Xin Y, Singh P, Wu F and Gao H 2022 *Interdiscip. Mater.* **1** 373–95
[32] Vaalma C, Buchholz D and Passerini S 2018 *Curr. Opin. Electrochem.* **9** 41–48
[33] Kim H, Seo D H, Urban A, Lee J, Kwon D H, Bo S H, Shi T, Papp J K, McCloskey B D and Ceder G 2018 *Chem. Mater.* **30** 6532–9
[34] Hironaka Y, Kubota K and Komaba S 2017 *Chem. Commun.* **53** 3693–6
[35] Zhang X, Wei Z, Dinh K N, Chen N, Chen G, Du F and Yan Q 2020 *Small* **16** 2002700
[36] Kim T, Choi W, Shin H C, Choi J Y, Kim J M, Park M S and Yoon W S 2020 *J. Electrochem. Sci. Technol.* **11** 14–25
[37] Augustyn V, Come J, Lowe M A, Kim J W, Taberna P L, Tolbert S H, Abruña H D, Simon P and Dunn B 2013 *Nat. Mater.* **12** 518–22
[38] Kim J, Park S, Hwang S and Yoon W S 2022 *J. Electrochem. Sci. Technol.* **13** 19–31
[39] He G, Bridges C A and Manthiram A 2015 *Chem. Mater.* **27** 6699–707
[40] Liao J, Hu Q, Che B, Ding X, Chen F and Chen C 2019 *J. Mater. Chem.* A **7** 15244–51
[41] Zhu Y, Qian Y, Ju Z, Ji Y, Yan Y, Liu Y and Yu G 2020 *ACS Nano* **14** 13824–33
[42] Beneš L, Melanova K, Svoboda J and Zima V 2012 *J. Incl. Phenom. Macrocycl. Chem.* **73** 33–53
[43] Zhu K, Sun Z, Liu P, Li H, Wang Y, Cao K and Jiao L 2021 *J. Energy Chem.* **63** 239–45
[44] Wu Y, Zong Q, Liu C, Zhuang Y, Tao D, Wang J, Zhang J, Zhang Q and Cao G 2023 *Small* **19** 2303227
[45] Jian X, Shen Q, Zhao X, Jin J, Wang Y, Li S, Qu X, Jiao L and Liu Y 2023 *Adv. Funct. Mater.* **33** 2302200
[46] Wan F, Zhang Y, Zhang L, Liu D, Wang C, Song L, Niu Z and Chen J 2019 *Angew. Chem., Int. Ed.* **58** 7062–7
[47] Ding J, Lin Y C, Liu J, Rana J, Zhang H, Zhou H, Chu I H, Wiaderek K M, Omenya F and Chernova N A 2018 *Adv. Energy Mater.* **8** 1800221
[48] Li J, Qi Y, Xiao F, Bao S and Xu M 2021 *Chem. Commun.* **57** 9566–9
[49] Wang Y, Feng Z, Cui P, Zhu W, Gong Y, Girard M A, Lajoie G, Trottier J, Zhang Q and Gu L 2021 *Nat. Commun.* **12** 13
[50] Zou J, Chen S, Wu Z, Gao J, Chen P, Ran Q, Li S, Wang L and Niu X 2020 *J. Power Sources* **480** 228864
[51] Kim H, Byeon Y W, Wang J, Zhang Y, Scott M C, Jun K, Cai Z and Sun Y 2022 *Energy Storage Mater.* **47** 105–12
[52] Nathan M G T, Park W B, Naveen N, Park S, Sohn K S and Pyo M 2020 *J. Electrochem. Soc.* **167** 100507
[53] Kumar P R, Kubota K, Miura Y, Ohara M, Gotoh K and Komaba S 2021 *J. Power Sources* **493** 229676